Effect of Simulation Methodology on Solder Joint Crack Growth Correlation

Robert Darveaux
1900 South Price Road
Chandler, AZ 85248
rdarv@amkor.com
Ph. 480-821-2408 ext 5235
Fax. 480-821-6730

Abstract

A generalized solder joint fatigue life model for surface mount packages was previously published in Refs [1,2]. The model is based on correlation to measured crack growth data on BGA joints during thermal cycling. It was subsequently discovered by Anderson et.al. that the ANSYS™ 5.2 finite element code used in the model had an error in its method for calculating plastic work [3]. It was shown that significant error in life prediction could result by using a recent version of the code where the bug has been fixed. The error comes about since the original crack growth constants were derived based on plastic work calculations that had the bug.

In this paper, crack initiation and growth constants are re-calculated using ANSYS™ 5.6. In addition, several other model related issues are explored with respect to the crack growth correlations. For example, 3D slice models were compared to quarter symmetry models. Anand's constitutive model was compared with Darveaux's constitutive model. It was shown that the crack growth rate dependence on strain energy density always had an exponent of 1.10 +/- 0.15. This is in the range of the original correlation, so the accuracy of *relative* predictions should still be within +/- 25%. However, the accuracy of *absolute* predictions could be off by a factor of 7 in the worst case, if the analyst uses a modeling procedure that is not consistent with that used for the crack growth correlation. The key to good accuracy is to maintain consistency in the modeling procedure.

Introduction

Analytical models in engineering have several practical uses: 1) rapid design optimization during the development phase of a product, 2) predicting field use limits, and 3) failure analysis of product returned from the field or failed in a qualification test. The solder joint fatigue model presented here was first published in Ref [1]. An outline of the procedure to predict fatigue life is shown schematically in Figure 1. The model utilizes finite element analysis to calculate the inelastic strain energy density accumulated per cycle during thermal or power cycling. The strain energy density is then used with crack growth data to calculate the number of cycles to initiate a cracks, and the number of cycles to propagate cracks through a joint.

In reference [2], more work was presented regarding sensitivity of the life prediction to the FEA procedure. As a result, the procedure was modified slightly to include volume averaging of the strain energy values near the joint interface. The model has been successfully applied to TSOP, CQFP, CBGA, PBGA, and power hybrid packages [1,2,4-9].

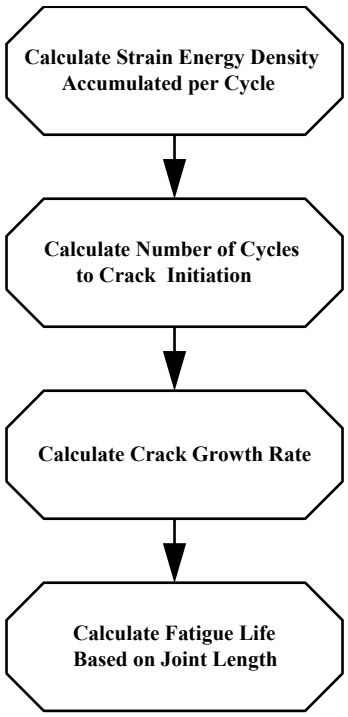

Figure 1. Solder joint fatigue life prediction method.

It was subsequently discovered by Anderson et.al. that ANSYS 5.5.2 and earlier versions of the finite element code had an error in their method for calculating plastic work [3]. Even though there had generally been good correlation to measured results, it was shown that significant error in life prediction could result by using a recent version of the code where the bug has been fixed (e.g. ANSYS 5.5.3 and later versions). The error comes about since the original crack growth constants were derived based on plastic work calculations that had the bug.

In this paper, crack initiation and growth constants are re-calculated using ANSYS 5.6. In addition, several other model related issues are explored with respect to the crack growth correlations. Several recommendations are made so the analyst can get accurate results more efficiently.

Constitutive Relations

Since solder is above half of its melting point at room temperature, creep processes are expected to dominate the deformation kinetics. Steady state creep of solder can be expressed by a relationship of the form [10-12]

$$\frac{d\varepsilon_s}{dt} = C_{ss}[\sinh(\alpha\sigma)]^n \exp\left(\frac{-Q_a}{kT}\right) \quad (1)$$

where $d\varepsilon_s/dt$ is the steady state strain rate, k is Boltzmann's constant, T is the absolute temperature, σ is the applied stress, Qa is the apparent activation energy, n is the stress exponent, α prescribes the stress level at which the power law dependence breaks down, and C_{ss} is a constant. Steady state creep data for 62Sn36Pb2Ag solder joints is shown in Figure 2.

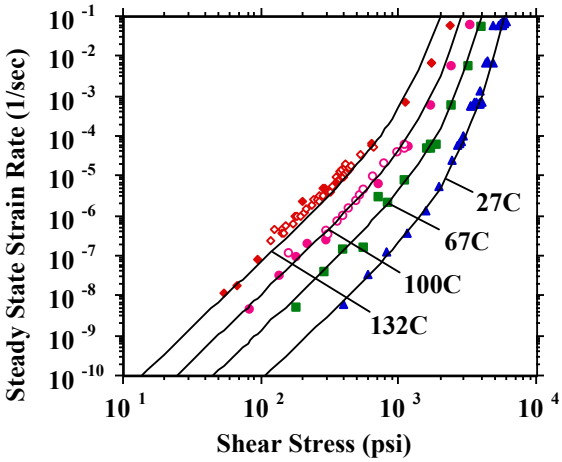

Figure 2. Steady state creep of 62Sn36Pb2Ag solder joints in shear with Cr/Ni/Au pad metallization.

Steady state creep is not generally achieved immediately when stress is applied. A certain amount of transient (or primary) creep occurs before attaining steady state. For normal decelerating transient creep, the strain rate starts high and decreases to the steady state value as the material work hardens. Transient creep at constant stress and temperature can be described by [13]

$$\varepsilon_c = \frac{d\varepsilon_s}{dt} t + \varepsilon_T \left(1 - \exp\left(-B\frac{d\varepsilon_s}{dt} t\right)\right) \quad (2)$$

where ε_c is the creep strain, $d\varepsilon_s/dt$ is the steady state creep rate, ε_T is the transient creep strain, and B is the transient creep coefficient. Taking the time derivative of both sides yields

$$\frac{d\varepsilon_c}{dt} = \frac{d\varepsilon_s}{dt}\left(1 + \varepsilon_T B \exp\left(-B\frac{d\varepsilon_s}{dt} t\right)\right) \quad (3)$$

where $d\varepsilon_c/dt$ is the instantaneous creep rate and $d\varepsilon_s/dt$ is the steady state creep rate. Hence at t = 0, the instantaneous creep rate is $(1 + \varepsilon_T B)$ times greater than the steady state creep rate, and after a long time, the instantaneous rate is equal to the steady state rate. A typical creep curve showing this behavior for 62Sn36Pb2Ag solder joints is shown in Figure 3 (γ is used to indicate shear strain, instead of ε for tensile strain).

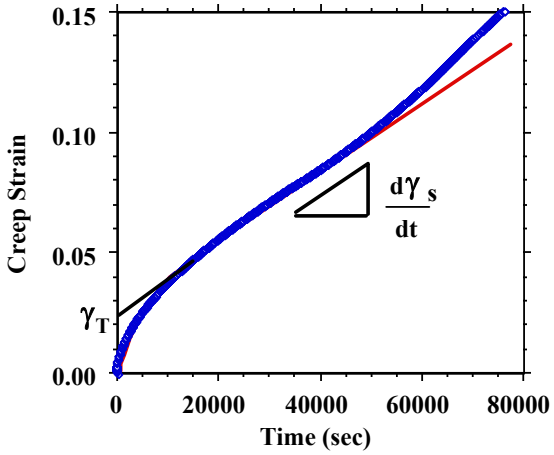

Figure 3. Typical creep strain plot for constant load test in shear.

At high stresses, $\tau/G > 10^{-3}$, there is also a time-independent plastic strain component to the deformation. The following strain hardening law can be used to describe high stress deformation

$$\varepsilon_p = C_p\left(\frac{\sigma}{G}\right)^{m_p} \quad (4)$$

where ε_p is the time-independent plastic strain, G is the shear modulus, and C_p and m_p are constants. The total inelastic strain is given by the sum of creep strain and plastic strain

$$\varepsilon_{in} = \varepsilon_c + \varepsilon_p \quad (5)$$

where ε_{in} is the total inelastic strain.

Equations (1) - (5) were shown to fit the deformation behavior of five different solder alloys in Ref [1]. The constants for 62Sn36Pb2Ag solder are given in Table 1. Unfortunately, these relations are not available in all commercial finite element codes as standard options. However, it is possible to input user defined constitutive relations in most codes.

Table 1.
Darveaux Model Constitutive Constants
62Sn36Pb2Ag Solder, Tensile

Parameter	Value	Definition
C_{SS} (1/sec)	8.03E4	Steady State Creep Prefactor
α (1/psi)	4.62e-4	Steady State Creep Power Law Breakdown
n	3.3	Steady State Creep Stress Exponent
Qa (eV)	0.70	Steady State Creep Apparent Activation Energy
ε_T	.023	Transient Creep Strain
B	263	Transient Creep Coefficient
C_p	3.35E11	Plastic Flow Prefactor
m_p	5.53	Plastic Flow Exponent

ANSYS does have viscoplastic elements as a standard option, but they use Anand's constitutive model [14,15]. The use of these elements is convenient since the user does not have to modify the source code. Anand's model is broken down into a flow equation, and three evolution equations:

Flow Equation

$$\frac{d\varepsilon_p}{dt} = A[\sinh(\xi\sigma/s)]^{1/m} \exp\left(\frac{-Q}{kT}\right) \qquad (6)$$

Evolution Equations

$$\frac{ds}{dt} = \{h_o(|B|)^a \frac{B}{|B|}\} \frac{d\varepsilon p}{dt} \qquad (7)$$

$$B = 1 - \frac{s}{s^*} \qquad (8)$$

$$s^* = s^\wedge \left[\frac{d\varepsilon_p / dt}{A} \exp\left(\frac{Q}{kT}\right)\right]^n \qquad (9)$$

In Ref[1], an approximate fit was made to the solder deformation data using only the flow equation, Eq. (6). In reference [2], a fit has been made using both the flow equation, Eq. (6), and the evolution equations, Eq. (7-9). A spreadsheet was set up to do 1-dimensional thermal cycle simulations, with assembly stiffness and imposed strain as inputs. Both the Anand model, Eqs. (6-9), and the Darveaux model, Eqs. (1-5), were used. An iterative process was used to determine the Anand constants that gave approximately the same results as the Darveaux model. The recommended Anand constants are listed in Table 2.

Table 2
Anand Constants for ANSYS
62Sn36Pb2Ag Solder

ANSYS	Parameter	Value	Definition
C1	S_o (psi)	1800	Initial Value of Deformation Resistance
C2	Q/k (1/K)	9400	Activation Energy / Boltzmann's Constant
C3	A (1/sec)	4.0E6	pre-exponential factor
C4	ξ	1.5	multiplier of stress
C5	m	.303	stain rate sensitivity of stress
C6	h_o (psi)	2.0E5	hardening constant
C7	s^ (psi)	2.0E3	coefficient for deformation resistance saturation value
C8	n	.07	Strain rate sensitivity of saturation (deformation resistance) value
C9	a	1.3	strain rate sensitivity of hardening

Non-linear Finite Element Analysis Method

Three-dimensional non-linear finite element modeling was used to calculate the strain energy density accumulation in solder joints. ANSYS 5.6 was used for all aspects: pre-processing, solution, and post-processing. The solder material was modeled as a viscoplastic solid, the printed circuit boards as orthotropic linear elastic solids, and the rest of the materials as linear elastic solids. The linear elastic material properties are given in Refs [1,16].

The goal of the simulations was to calculate the plastic work per unit volume (or viscoplastic strain energy density) accumulated per thermal cycle. Either two or three complete thermal cycles were simulated in order to establish a stable stress-strain hysteresis loop. The plastic work accumulated during the last cycle was used for all crack growth correlations. A typical slice model is shown in Figure 4, and a quarter symmetry model is shown in Figure 5. A solder joint model is shown in Figure 6.

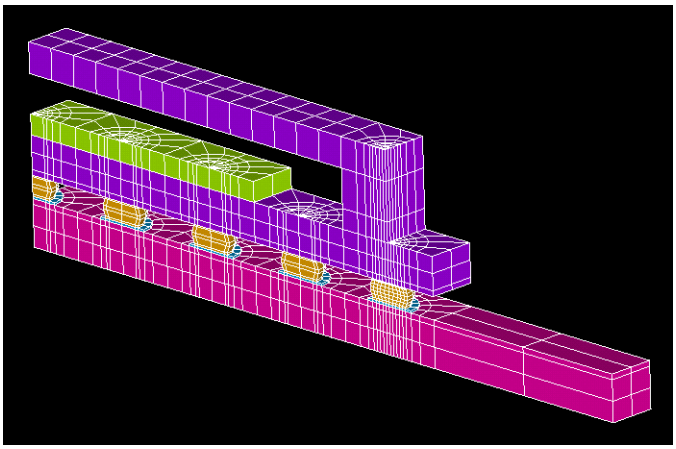

Figure 4. Slice model of CBGA assembly

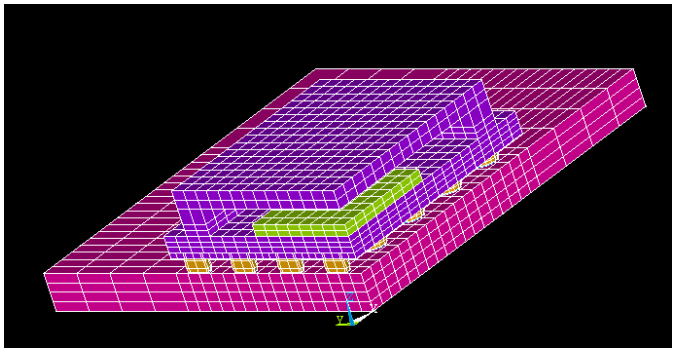

Figure 5 Quarter symmetry model of CBGA assembly

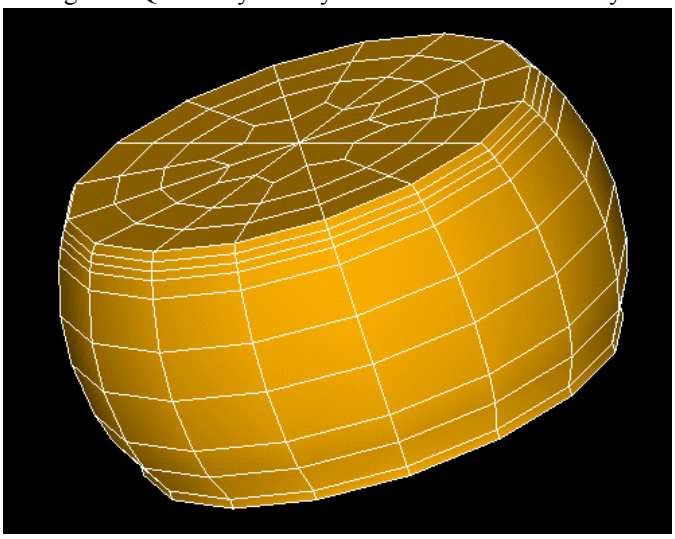

Figure 6. Model of solder joint. Three layers near substrate interface are .0005" thick each.

The slice model (Figure 4) has a symmetry boundary condition along the centerline of the joints. The boundary condition along the opposite edge (centerline between rows) is coupled in the y-direction.

It was shown in Ref [2] that the calculated strain energy density increases as element size in the solder joint decreases. Hence, a volume averaging technique was used to reduce this sensitivity to meshing. The strain energy value of each element is normalized by the volume of the element.

$$\Delta W_{ave} = \frac{\sum \Delta W \bullet V}{\sum V} \qquad (10)$$

where ΔW_{ave} is the average viscoplastic strain energy density accumulated per cycle for the interface elements, ΔW is the viscoplastic strain energy density accumulated per cycle of each element, and V is the volume of each element. This technique helps make the analysis more robust, but it was found that there was still some dependency on the thickness of the interface elements. For the models in the present study, the thickness of the first three layers of elements was set to 0.0005 inches each.

Regarding time step size, sub-steps that result in a 10C temperature change during the ramps, and an increasing time step during the dwells were used. For example, considering a -40C <-> 125C thermal cycle with 900 sec ramps and 900 sec dwells, sixteen load steps were used during the ramps, and 4 load steps during the dwells (60, 120, 240, and 480 sec).

Linear + Non-linear Analysis Method

A second method was employed to calculate the strain energy density accumulation in solder joints. In this method, linear finite element analysis is used to calculate the assembly stiffness and imposed strain on the solder joints. Then a 1-dimensional nonlinear analysis is used to calculate strain energy density accumulated per cycle. The non-linear simulation can be performed in a spreadsheet. This method was used to analyze flip chip assemblies in Ref [17].

Two finite element simulations are required. The reference temperature is set to the high temperature of the cycle, and the final temperature is set to the average temperature of the cycle. For example, for a –40C ⇔ 125C cycle, the reference temperature would be 125C and the final temperature is 42.5C. A linear analysis is used to calculate the equivalent stress and strain distribution in the solder joints. This simulation is then repeated using a 100X lower elastic modulus for the solder material. The results of these two simulations are used to estimate the effective assembly stiffness, S_e , and imposed strain per degree temperature change, ε_o , as indicated in Figure 7.

$$S_e = -(\sigma_1 - \sigma_{.01})/(\varepsilon_1 - \varepsilon_{.01}) \qquad (11)$$

$$\varepsilon_o = (\varepsilon_{.01} + \sigma_{.01}/S_e)/\Delta T \qquad (12)$$

where σ_1 and ε_1 are the equivalent stress and strain calculated using the full elastic modulus of solder, and $\sigma_{.01}$ and $\varepsilon_{.01}$ are calculated using 1/100 the elastic modulus of solder.

The advantage of this method is that it is at least 30 times faster than doing a full non-linear finite element analysis. The disadvantages are 1) the full effect of temperature dependent properties cannot be captured, and 2) the stress distribution in the solder joints is probably not exactly equal to that of a full non-linear method.

Crack Growth Measurement

A series of tests were run using 4 assemblies, 2 alloys, and 8 thermal cycle conditions. All of the assemblies used ceramic chip carriers and eutectic ball grid array joints, but there were variations in the PC boards, chip carrier structures, and joint array patterns. Details of the Ceramic BGA assemblies are given in Table 3. Thermal cycling conditions are given in Table 4. All of the tests were conducted using 62Sn36Pb2Ag, and 3 additional tests were done using 60Sn40Pb.

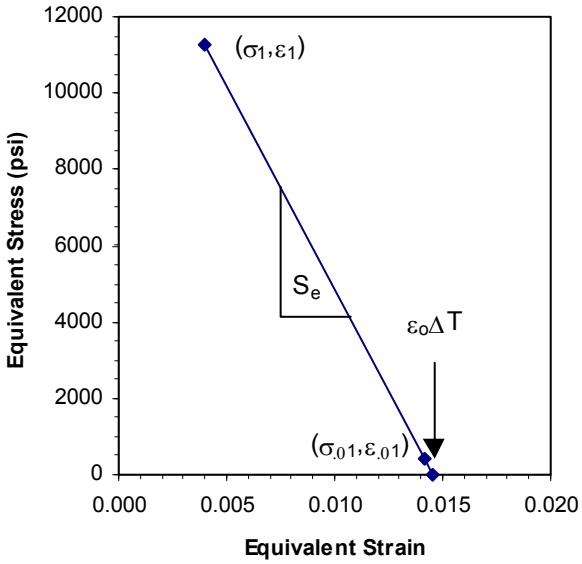

Figure 7. Graphical representation of effective assembly stiffness and imposed strain calculated using linear finite element simulations.

The dye-n-pry technique was used to measure crack length throughout the thermal cycle tests [1,18]. Each test was divided into 6 to 8 intervals, and 3 chip carriers were pried off at each interval. The primary and secondary crack lengths were measured along lines extending from the package neutral point to the 8 outermost joints. Hence, a total of 24 joints were measured to determine each crack length data point.

Representative crack growth data are shown in Figure 8. The crack growth rate (slope of the curves) stays essentially constant during the thermal cycle tests. The number of cycles to crack initiation can be determined by extrapolating the curves back to the x-axis (crack length = 0). It is seen that crack initiation only accounts for about 10% of the fatigue life for these particular assemblies.

Given in Table 5 are the combined primary + secondary crack length data. The combined data are presented because our intention is to correlate with strain energy density values that were calculated by averaging across all the elements at the joint interface. Note that these are characteristic (63.2 percentile) crack rate data as calculated by a 3-parameter Weibull analysis of 1/length for each set of 24 readings [1]. In contrast, the original crack rate data given in Ref [18] were simply derived from the mean values of the crack length data. Hence, there is not quite exact agreement between the present work and Ref [18].

Crack Growth Correlations

In this section, the measured crack growth data are correlated with calculated inelastic strain energy density per cycle in the solder. The various terminology that is equivalent to "inelastic" are "viscoplastic" for the Anand constitutive model, "time-independent plastic + time-dependent creep" for the Darveaux constitutive model, or "plastic work per unit volume" in the ANSYS code. Several different modeling methodologies were used.

In each case, the crack growth data were fit to relations of the form

$$\text{Crack Initiation:} \quad N_O = K_1 \, \Delta W_{ave}^{\ K_2} \qquad (13)$$

$$\text{Crack Growth:} \quad \frac{da}{dN} = K_3 \, \Delta W_{ave}^{\ K_4} \qquad (14)$$

Shown in Table 6 are the constants K_1, K_2, K_3, and K_4 for all the various modeling methodologies employed. The finite element model configuration, simulation method, and constitutive models are described in previous sections. It was found that the TUNIF temperature change command in ANSYS does not give a ramped loading. This reduces accuracy somewhat, and can cause convergence problems as well. The BF command is preferred.

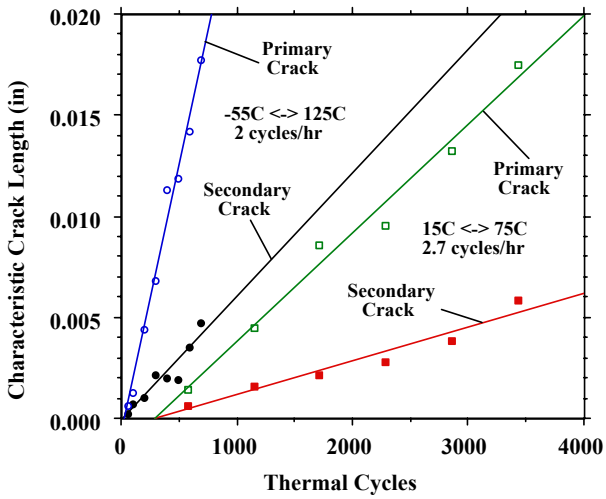

Figure 8. Crack growth data for data sets 5 and 6.

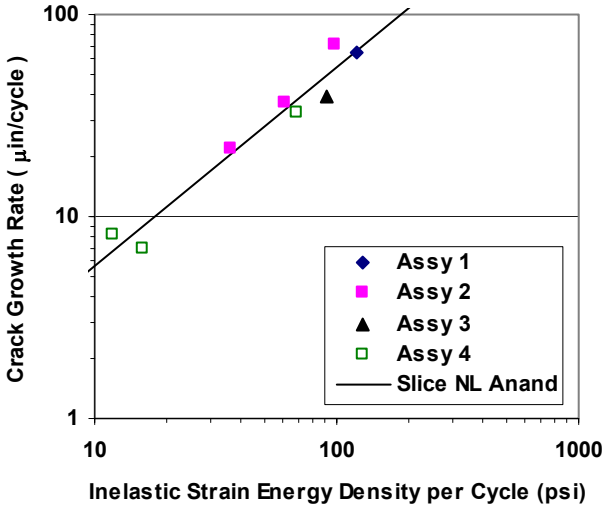

Figure 9. Crack growth rate correlation. Slice, non-linear FEA, Anand constitutive model. Averaging over element layers 1+2, .001" total thickness.

Table 3.
Ceramic BGA Assemblies for Crack Growth Study

Assembly	PC Board	Substrate	Die	Cover	Solder Joints
1	6 Layer PI .037 thick	Co-fired $A1_2O_3$ .560 x .630 x .028	.248 x .291 x .015	.500 x .560 x .064	8 x 9, no corners .030 dia .070 pitch .0146 high
2	6 Layer PI .037 thick	Co-fired $A1_2O_3$ .560 x .630 x .028	none	none	8 x 9, no corners .030 dia .070 pitch .0168 high
3	2 Layer FR4 .050 thick	Co-fired $A1_2O_3$ .560 x .630 x .028	. 248 x .291 x .015	.500 x .560 x .064	8 x 9, no corners .030 dia .070 pitch .0168 high
4	2 Layer PI .038 thick	Thin Film $A1_2O_3$ .680 x .680 x .025	none	.570 x .570 x .064	10 x 10, no corners .030 dia .060 pitch .0185 high

1) All dimensions in inches.

Table 4.
Thermal Cycle Conditions for Crack Growth Study

Data Set	Assembly	Alloy	Low Temp (°C)	High Temp (°C)	Ramp Time Up (sec)	Dwell Time High (sec)	Ramp Time Down (sec)	Dwell Time Low (sec)
1	2	62Sn36Pb2Ag	-30	125	300	600	500	600
2	1	62Sn36Pb2Ag	-40	85	450	1350	700	1100
3	2	62Sn36Pb2Ag	-55	125	30	280	90	220
4	2	62Sn36Pb2Ag	-5	96	210	600	270	540
5	4	62Sn36Pb2Ag	-55	125	450	450	700	200
6	4	62Sn36Pb2Ag	15	75	120	540	180	480
7	3	62Sn36Pb2Ag	-40	100	600	1200	900	900
8	4	62Sn36Pb2Ag	25	75	600	21000	3600	18000

Table 5.
Measured Crack Growth Data
Combined Primary + Secondary Crack Length

Data Set	Crack Initiation (cycles)	Crack Growth Rate (µin/cycle)
1	81.1	36.3
2	21.1	65.0
3	48.3	71.7
4	130	21.5
5	29.1	32.7
6	289	6.87
7	3.9	39.6
8	500	8.18

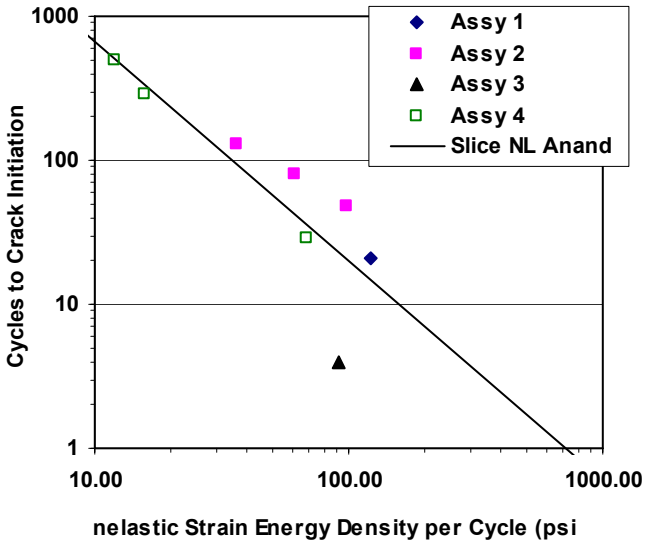

Fi
FEA, Anand constitutive model. Averaging over element layers 1+2, .001" total thickness.

Table 6
Crack Growth Correlation Constants

Finite Element Model Config	Simulation Method	Constitutive Model	ANSYS Version	Temperature Change Command	Time Step Scheme	Thickness Of Element Layers in Averaging (10^{-3} in)	K_1 (cycles/psi^{K_2})	K_2	K_3 (10^{-7} in/cycle/psi^{K_4})	K_4
Slice	NL FEA	Anand	5.2	TUNIF	Coarse	0.6	26800	-1.44	1.92	1.15
						1.0	21800	-1.45	2.41	1.15
						1.3	18100	-1.46	2.77	1.15
Slice	NL FEA	Anand	5.6	TUNIF	Coarse	1.0	19500	-1.51	6.19	0.98
Slice	NL FEA	Anand	5.6	BF	Coarse	1.0	20300	-1.52	6.03	0.99
Slice	NL FEA	Anand	5.6	BF	Fine	1.0	22400	-1.52	5.86	0.98
QTR	NL FEA	Anand	5.6	BF	Fine	0.5	71000	-1.62	2.76	1.05
						1.0	56300	-1.62	3.34	1.04
						1.5	48300	-1.64	3.80	1.04
QTR	L + NL	Anand	5.6	BF	Fine	0.5	58800	-1.49	1.29	1.16
						1.0	67500	-1.54	1.20	1.19
						1.5	71900	-1.58	1.16	1.21
QTR	L + NL	Darveaux	5.6	BF	Fine	0.5	69900	-1.55	1.19	1.19
						1.0	84200	-1.61	1.08	1.23
						1.5	91000	-1.65	1.04	1.25

Shown in Figure 9 is the crack growth rate correlation using a slice non-linear finite element model with Anand's constitutive model. The strain energy density values were averaged over first two element layers next to the package interface. The total thickness of these two layers is .001". The data points representing each test assembly from Table 3 are shown. All of the assemblies follow approximately the same trend line.

Shown in Figure 10 is the correlation with crack initiation. Typically, the data for crack initiation is a little more scattered than that for crack growth.

Shown in Figures 11 – 13 are the crack growth correlations using quarter symmetry finite element models. Comparing Figure 9 to Figure 11, it is seen that slice model and quarter symmetry model give approximately the same relative relation between the 4 assemblies. The position of each assemblies data relative to the trend line is similar in Figures 9 and 11. On the other hand, comparing Figure 11 to Figures 12 and 13, it is seen that the linear finite element analysis + 1-D nonlinear method gave somewhat different results than the nonlinear finite element method. In Figures 12 and 13, assembly 2 data has shifted to the right of the tend line, and assemblies 1 and 3 data have shifted to the left. Assemblies 1 and 3 should have the highest stiffness since they both have a die and a cover attached to the substrate. This shift in data relative to the trend line suggests that the 2 different modeling methodologies do not capture this change in stiffness equally.

Since the data in Figures 12 and 13 are similar to each other, it appears that the 2 constitutive models produce similar results.

Shown in Figure 14 are crack growth correlation trend lines drawn by averaging 1, 2, and 3 layers of elements near the substrate interface. Quarter symmetry, non-linear finite element analysis was used. It is seen that the slope of the curves is essentially the same, they are just offset in the horizontal direction. Since the slopes are consistent (K_4 = 1.04 to 1.05), relative fatigue life predictions should be somewhat independent of the averaging scheme chosen.

Note in Table 6 that the constant K_4 does vary a little more with element averaging scheme for the linear FEA + 1-D non-linear method. The range in K_4 is 1.16 to 1.21 for the Anand constitutive model and 1.19 to 1.25 for the Darveaux constitutive model. This confirms that linear finite element analysis does not capture the stress and strain concentration near the interface the same as non-linear finite element analysis.

Shown in Figure 15 is a comparison of the 7 different methods used to generate crack growth rate correlations. The highlighted region indicates the range of measured data. The trend lines are extrapolated above and below this region to amplify any divergence between curves.

It is seen that the curves tend to diverge at the low strain energy density end of the scale. This region would be representative of very mild cycling, possibly field use conditions (hopefully field use conditions!).

The divergence between curves is almost 7X in comparing the worse case between a slice non-linear finite element model and a quarter symmetry linear + 1-D non-linear model. Hence, if an analyst used the crack growth correlation constants from the slice model and tried to apply them to a quarter symmetry linear + 1-D non-linear analysis, the error in field use extrapolations could be up to 7X.

This example clearly highlights the requirement of consistency. If an analyst is using a slice model, then the slice model correlation constants should be used as well. Also, if there is any measured life data available, an analyst will typically make relative predictions. In this case the error will be significantly less.

There is no way to determine from the work presented here which methodology or which correlation is "correct". There are a couple of possible approaches one could use to answer this question. One could use Moiré or strain gage techniques to measure strains in the PCB and package to establish further correlation to the simulation results. Alternatively, the various methods could also be applied to a large database of measured life test results to see which method does the best job of predicted life.

On purely theoretical grounds, one would expect the quarter symmetry models to be more accurate, because a slice model cannot capture the effects at the die and package corners. Joints in these regions typically fail first BGA assemblies.

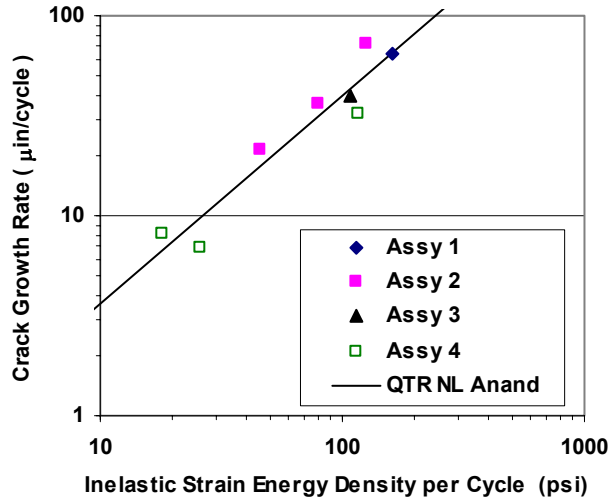

Figure 11. Crack growth rate correlation. Quarter symmetry, non-linear FEA, Anand constitutive model. Averaging over element layers 1+2, .001" total thickness.

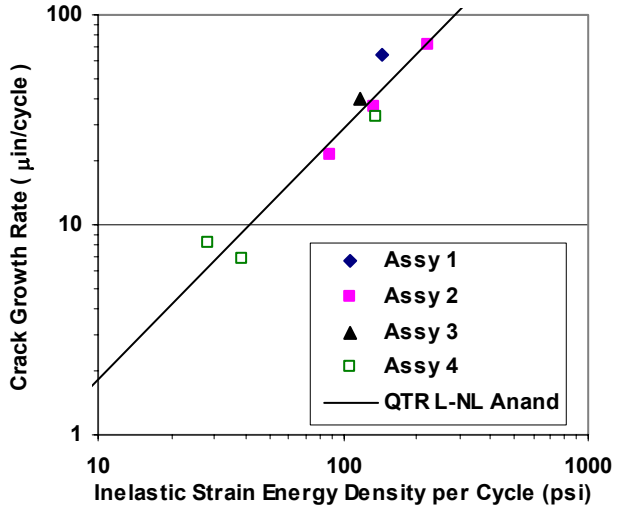

Figure 12. Crack growth rate correlation. Quarter symmetry, linear FEA + 1D non-linear, Anand constitutive model. Averaging over element layers 1+2, .001" total thickness.

In comparing ANSYS 5.6 to 5.2, it is seen that version 5.6 predicts lower strain energy density for a given simulation. This is consistent with the finding of Anderson et.al. [3], who originally found the bug in ANSYS 5.2.

Just by coincidence, the crack growth correlation for ANSYS 5.6 quarter symmetry model is very close the original correlation for ANSYS 5.2 slice model. Hence, for an analyst using the newer version of code, it is possible that the error was fairly small if they happened to be utilizing a quarter symmetry model.

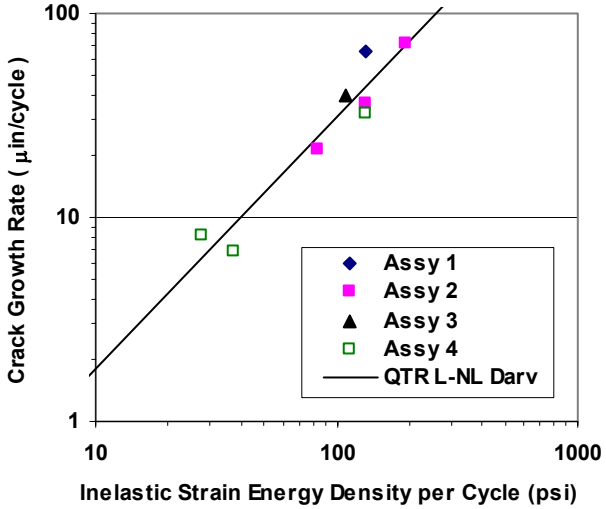

Figure 13. Crack growth rate correlation. Quarter symmetry, linear FEA + 1D non-linear, Darveaux constitutive model. Averaging over element layers 1+2, .001" total thickness.

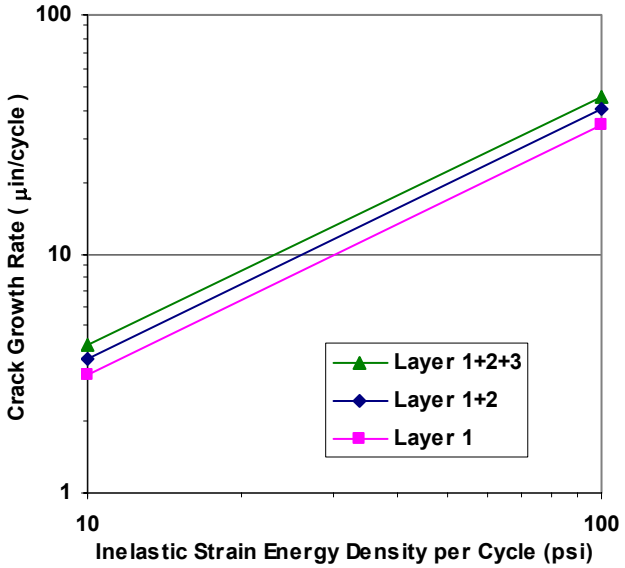

Figure 14. Crack growth rate correlations. Quarter symmetry, non-linear FEA, Anand constitutive model. Comparison of element layer averaging schemes.

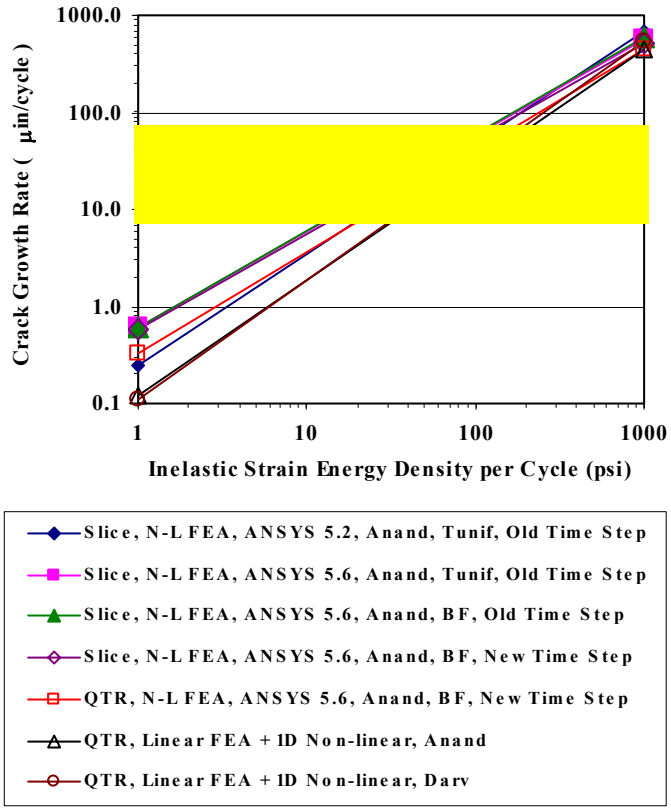

Figure 15. Crack growth rate correlations. Comparison of modeling methodologies. Highlighted region indicates range of measured data.

Fatigue Life Prediction

To predict fatigue life from crack growth data, one needs to assume a certain failure distribution. Clech [19] has shown that a 3-parameter Weibull distribution is most appropriate. The cumulative distribution of failures, F, for the 3P Weibull distribution is given by

$$F = 0 \qquad \text{for } N < N_{ff}$$

$$F = 1 - \exp\left[-\left(\frac{N - N_{ff}}{\alpha_w - N_{ff}}\right)^{\beta_w}\right] \qquad \text{for } N > N_{ff} \qquad (15)$$

where N is the number of cycles, N_{ff} is the failure free life, α_w is the characteristic life at which 63.2% of the population has failed, and β_w is the shape parameter which indicates the amount of scatter in the data.

Since the crack growth rate was shown to be constant during thermal cycling, the fatigue life of a joint can be calculated by adding the number of cycles for crack initiation plus the number of cycles to grow the cracks across the joint interface. The characteristic life is given by

$$\alpha_w = No + \frac{a}{da / dN} \qquad (16)$$

where "a" is the joint diameter at the interface (final crack length). It was shown in Ref [1] that the maximum crack length in the population was approximately 2X the characteristic length. Hence we would expect the failure free life to be approximately one half of the characteristic life

$$N_{ff} = \alpha_w / 2 \qquad (17)$$

In practice, one does not test an infinitely large sample size, so the number of cycles to first failure will be greater than the failure free life. The cycles to first failure is given by

$$N = N_{ff} + (\alpha_w - N_{ff})(-\ln(1-F))^{1/\beta_w} \qquad (18)$$

where the F is calculated in terms of median rank

$$F = (1 - 0.3) / (S_s + 0.4) \qquad (19)$$

where S_s is the sample size. For example, a typical test has a sample size of 32 units. The first unit to fail represents a cumulative fraction failed of 0.0216 (or 2.16%).

The procedure to calculate fatigue life consists of the following steps

1] Calculate inelastic strain energy density per cycle using one of the methods described in previous sections.
2] Calculate number of cycles to crack initiation using Eq. (13) and Table 6, using the correct constants for the method that was utilized.
3] Calculate crack growth rate using Eq. (14) and Table 6, using the correct constants for the method that was utilized.
4] Calculate characteristic life based on Eq. (16).
5] Calculate failure free life based on Eq. (17).
6] Calculate the first failure for a particular sample size based on Eqs. (18) and (19).

As an example, consider the following prediction for a 144 tfBGA. A quarter symmetry, non-linear finite element model was used with Anand's constitutive model. The thermal cycle was -40C <=> 125C, with 900 sec ramps and 900 sec dwells. 16 load steps were used during the ramps, and 4 load steps during the dwells (60, 120, 240, and 480 sec). The simulation results show that the worst case joint is under the die edge. Moreover, the interface at the package side has the highest inelastic strain energy density per cycle. The solder element thickness at this interface was 0.0005", and the interface diameter was 0.016". The shape factor, β_w, was assumed to be 2.6. A summary of the calculation results is shown in Table 7.

Table 7
Fatigue Life Prediction Example

ΔW (psi)	No (cycles)	da/dN (in/cycle)	Nff (cycles)	First Fail (cycles)	α (cycles)
33.0	246	1.08E-5	861	1058	1721

Relative vs. Absolute Predictions

A comment should be made about *relative* versus *absolute* predictions. In most cases, there is at least one data set of measured fatigue life for a particular package assembly. In this scenario, *relative* predictions can be made. The procedure is to first calculate life for the known case (measured data), then calculate life for the unknown case. A relative life prediction can be made from these two calculations. For example, the unknown case could be changing motherboard thickness, pad diameter, ball size, etc. The accuracy of relative predictions is usually in the range of +/- 25% or better [1,2,3-9].

For the case where the package assembly is only in the concept stage, and there is no measured data available, *absolute* predictions must be made. Also, if one is comparing measured versus predicted results for a wide range of package types, material sets, and test conditions, the prediction is more of an absolute nature. For absolute predictions, the accuracy is somewhat less, but typically +/- 2X or better. If one does a very good job at characterizing the material properties and modeling the exact configuration that was tested, the accuracy can be better than +/- 2X. For example, a quarter or eighth symmetry model should be better than a slice model in this regard.

One of the reasons that reasonable prediction accuracy was possible with earlier versions of ANSYS that had a bug in the plastic work calculation was that this error carried through from simulation to simulation. In a relative sense, the error washed out. However, when the recent version of ANSYS was released where the bug was fixed, the error no longer carried through from the original crack growth correlation. The error no longer washed out.

Effect of Multiple Joints

In Refs [1,20] the argument was made that the fatigue life of a component should be related to the number of solder joints, because they are all acting in series and the failure of any one joint will cause failure of the component. Hence, the overall component reliability, R_c, is related to the joint reliability, R_j, by

$$R_c = \prod R_j \qquad (20)$$

The number of cycles that R_c of the components survive is given by [1]

$$N_c = N_{ff} + (\alpha_j - N_{ff})\left(\frac{-\ln(R_c)}{q}\right)^{1/\beta_w} \qquad (21)$$

where α_j is the characteristic life of the joints and q is the number of joints. Not all of the joints are subjected to identical stress, so the component needs to be divided into groups of joints that have similar stress applied. This procedure was demonstrated in Ref [1].

For components with hundreds of joints, the reliability of the component will be significantly de-rated compared to that of an individual joint. It is questionable whether such a large de-rating if valid.

In reality, the joints that are most likely to fail are almost always near the corners of the die or corners of the package. If one does a lot of failure analysis after thermal cycling, this trend becomes evident. This is not to say that failures do not occur in the middle region of a row of joints, but rather that the vast majority of failures occur at the corners. Hence, it is probably not valid to consider all of the joints when de-rating component reliability.

This issue is relevant in the present life prediction methodology because crack growth data from individual joints is being used to predict life of components with many joints. If we consider the group of worst case joints to control the component reliability, then Eq. (21) can combined with Eq. (17) and re-arranged to give the de-rating factor for a component

where α_c is the characteristic life of the component, α_j is the characteristic life of the worst case joints, and q is the number of worst case joints, typically 4 or 8.

$$\frac{\alpha_c}{\alpha_j} = \frac{1}{2}\left(1 + \left(\frac{1}{q}\right)^{1/\beta_w}\right) \qquad (22)$$

An alternate approach to Eq. 22 is to consider all of the highest stressed joints on a component as an individual Weibull distribution. Hence, if simulation results predict that the joints at the package corners are most likely to fail first, then the component failure will occur when 1 out of a population of 4 corner joints fails. To estimate the de-rating factor for this approach, Eqs. (17) to (19) can combined and re-arranged to give

$$\frac{\alpha_c}{\alpha_j} = \frac{1}{2}\left[1 + \left[-\ln\left(1 - \left(\frac{.7}{q + .4}\right)\right)\right]^{1/\beta_w}\right] \qquad (23)$$

Plots of component de-rating factor, α_c / α_j, for both Eqs. (22) and (23) are shown in Figure 16 (β_w was assumed to be 2.6). It is seen that for typical case of 4 worst case joints, the de-rating factor is 0.79 for Eq. (22) and 0.75 for Eq. (23). Hence, the component characteristic life should be 75% to 79% of the characteristic life calculated for the worst case joints. Note that the de-rating factor approaches 0.5 for a large number of joints. In this limit, the characteristic life of the component is equal to the failure free life of the component (which is equal to the failure free life of the joints).

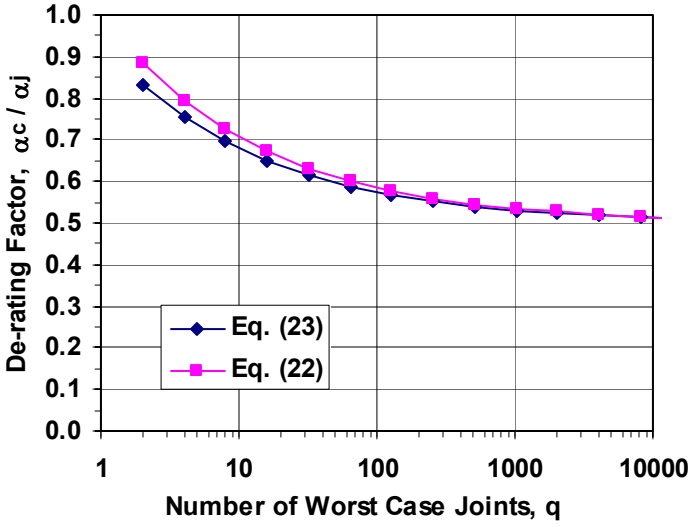

Figure 16. De-rating factor for component based on number of worst case joints.

Conclusions

1) Crack initiation and growth correlations were re-established using measured crack growth data and ANSYS 5.6 simulation results.

2) Three simulation methodologies and two constitutive models were compared with respect to their impact on the crack growth correlations.

3) The crack growth rate dependence on strain energy density always had an exponent of 1.10 +/- 0.15. This is in the range of the original correlation, so the accuracy of relative predictions should still be within +/- 25%.

4) The accuracy of absolute predictions could be off by a factor of 7 in the worst case, if the analyst uses a modeling procedure that is not consistent with that used for the crack growth correlation

5) De-rating factor relations were derived to estimate component fatigue life based on worst case joint fatigue life.

Acknowledgments

The author would like to acknowledge helpful discussions with Zane Johnson regarding temperature change commands in ANSYS.

References

1] R. Darveaux, K. Banerji, A. Mawer, and G. Dody, "Reliability of Plastic Ball Grid Array Assembly," Ball Grid Array Technology, J. Lau Editor, McGraw-Hill, Inc., New York, 1995.

2] R. Darveaux, "Solder Joint Fatigue Life Model," Proc TMS, 1997.

3] T. Anderson, I. Guven, E. Madenci, and G. Gustafsson, "The Necessity of Reexamining Previous Life Prediction Analyses of Solder Joints in Electronic Packages," Proc 1999 ECTC.

4] R. Darveaux, "Optimizing the Reliability of Thin Small Outline Package (TSOP) Solder Joints," Advances in Electronic Packaging 1995 - Proc. ASME Interpack '95, pp. 675-685.

5] A. Mawer, J. Trent, N. Vo, T. Vo, Y. Guo, P, Seto, L. Bosley, and R. Darveaux, "Reliability Evaluation of a PBGA MCM for Automotive Applications," Proc SMI 1997, pp. 125-132.

6] A. Mawer, D. Cho, and R. Darveaux, "The Effect of PBGA Solder Pad Geometry on Solder Joint Reliability," Proc. SMI, 1996, pp. 127-135.

7] J. Fusaro and R. Darveaux, "Reliability of Copper Baseplate High Current Power Modules," Proc. 1996 ISHM Symposium.

8] M. Amagai, "Chip Scale Package (CSP) Solder Joint Reliability and Modeling," Proc. 36th International Reliability Physics Symposium, 1998, pp. 260-268.

9] Z. Johnson, "Implementation of and Extensions to Darveaux's Approach to Finite-Element Simulation of BGA Solder Joint Reliability," Proc. 1999 ECTC.

10] F. Garfalo, *Fundamentals of Creep and Creep-Rupture in Metals*, The Macmillan Company, New York, NY, 1965.

11] K.L. Murty and I. Turlik, "Deformation Mechanisms in Lead-Tin Alloys, Application to Solder Reliability in Electronic Packages," Proceedings 1st Joint Conference on Electronic Packaging, ASME/JSME, 1992, pp. 309-318.

12] H.J. Frost and M.F. Ashby, *Deformation Mechanism Maps*, Pergamon Press, 1982, Chapter 2.

13] K.L. Murty, G.S. Clevinger, and T.P. Papazoglou, "Thermal Creep of Zircaloy-4 Cladding," Proceedings 4th International Conference on Structural Mechanics in Reactor Technology, C 3/4, 1977.

14] L. Anand, "Constitutive Equations for Hot-Working of Metals," International Journal of Plasticity, Vol. 1, pp. 213-231, 1985.

15] S.B. Brown, K.H. Kim, and L. Anand, "An Internal Variable Constitutive Model for Hot Working of Metals," International Journal of Plasticity, Vol. 5, pp. 95-130, 1989.

16] R. Darveaux and A. Mawer, "Thermal and Power Cycling Limits of Plastic Ball Grid Array (PBGA) Assemblies," Proc. Surface Mount International, 1995, pp. 315-326.

17] R. Darveaux and K. Banerji, "Fatigue Analysis of Flip Chip Assemblies Using Thermal Stress Simulations and a Coffin-Manson Relation," Proc. 41st IEEE ECTC, 1991, pp. 797-805.

18] R. Darveaux, "Crack Initiation and Growth in Surface Mount Solder Joints," Proc. ISHM International Symposium on Microelectronics, 1993, pp.86-97.

19] J-P. Clech, D.M. Noctor, J.C. Manock, G.W. Lynott, and F.E. Bader, "Surface Mount Assembly Failure Statistics and Failure Free Time," Proc. 44th IEEE ECTC, 1994.

20] A. Mawer and R. Darveaux, "Calculation of Thermal Cycling and Application Fatigue Life of Plastic Ball Grid Array (PBGA) Package," Proc. IEPS, 1993.